THE JOURNAL OF BIOLOGICAL CHEMISTRY VOL. 287, NO. 26, pp. 21741–21750, June 22, 2012

The Contribution of RCK Domains to Human BK Channel Allosteric Activation*[S]

Received for publication, January 24, 2012, and in revised form, April 10, 2012 Published, JBC Papers in Press, May 3, 2012, DOI 10.1074/jbc.M112.346171

Nicoletta Savalli[‡], Antonios Pantazis[‡], Taleh Yusifov[‡], Daniel Sigg[‡], and Riccardo Olcese[‡§¶1]

From the [‡]Department of Anesthesiology, Division of Molecular Medicine, the [§]Brain Research Institute, and the [¶]Cardiovascular Research Laboratories, David Geffen School of Medicine, University of California at Los Angeles, Los Angeles, California 90075

Background: In BK channels, Ca^{2+} and voltage sensors are allosterically connected to the pore.
Results: We optically resolved voltage sensor rearrangements, initiated by Ca^{2+} binding to the intracellular domains RCK1 and RCK2. Impairing the RCK2 abolished this allosteric effect.
Conclusion: The RCK2 Ca^{2+} sensor is required for the allosteric facilitation of voltage sensor activation.
Significance: RCK1 and RCK2 Ca^{2+} sensors are not functionally homologous.

Large conductance voltage- and Ca^{2+}-activated K^+ (BK) channels are potent regulators of cellular processes including neuronal firing, synaptic transmission, cochlear hair cell tuning, insulin release, and smooth muscle tone. Their unique activation pathway relies on structurally distinct regulatory domains including one transmembrane voltage-sensing domain (VSD) and two intracellular high affinity Ca^{2+}-sensing sites per subunit (located in the RCK1 and RCK2 domains). Four pairs of RCK1 and RCK2 domains form a Ca^{2+}-sensing apparatus known as the "gating ring." The allosteric interplay between voltage- and Ca^{2+}-sensing apparati is a fundamental mechanism of BK channel function. Using voltage-clamp fluorometry and UV photolysis of intracellular caged Ca^{2+}, we optically resolved VSD activation prompted by Ca^{2+} binding to the gating ring. The sudden increase of intracellular Ca^{2+} concentration ($[Ca^{2+}]_i$) induced a hyperpolarizing shift in the voltage dependence of both channel opening and VSD activation, reported by a fluorophore labeling position 202, located in the upper side of the S4 transmembrane segment. The neutralization of the Ca^{2+} sensor located in the RCK2 domain abolished the effect of $[Ca^{2+}]_i$ increase on the VSD rearrangements. On the other hand, the mutation of RCK1 residues involved in Ca^{2+} sensing did not prevent the effect of Ca^{2+} release on the VSD, revealing a functionally distinct interaction between RCK1 and RCK2 and the VSD. A statistical-mechanical model quantifies the complex thermodynamics interplay between Ca^{2+} association in two distinct sites, voltage sensor activation, and BK channel opening.

Allostery is an intrinsic property of all proteins that allows distant sites to be energetically coupled, resulting in the mutual and efficient regulation of many biological processes (1, 2). Allostery can originate from binding events, covalent modifications, mutations, or changes in the environment. In ion channels, the gating mechanism(s) rely on the allosteric coupling between the pore and other modulatory domains, specialized to sense different stimuli, such as changes in membrane potential, temperature, mechanical stress, and the concentration of signaling molecules. Although the available atomic structures of ion channels or their functional domains are rapidly increasing, the mechanisms underlying allostery in these proteins are far from being fully understood. Several studies have provided experimental evidence of cooperative interactions in K^+ channels (3–8). An example of a highly allosteric membrane protein is the large conductance, voltage- and Ca^{2+}-activated (BK, Slo1) K^+ channel. BK channel open probability (P_o) is controlled by cooperative interactions between its four transmembrane voltage-sensing domains (VSDs),[2] an intracellular multiligand-sensing domain (gating ring), and the pore (6, 9–12) (Fig. 1*A*). Functional BK channels are tetrameric proteins (13), each subunit composed of seven transmembrane segments (S0–S6) and a large intracellular C terminus (14). As typical of voltage-activated K^+ channels (15), the transmembrane region of BKchannels includes helices S5-S6, which contribute to the central, K^+-selective pore domain and a VSD including the charge-bearing segments S2-S3-S4 (16–20) (Fig. 1*A*). BK sensitivity to Ca^{2+} and other intracellular ligands (Mg^{2+}, H^+, CO, Heme, etc.) is conferred by the large intracellular C-terminal region (10, 11, 21), which encompasses two tandem regulator of conductance of K domains, RCK1 and RCK2 (22–29) (Fig. 1). RCK1 includes residues involved in both high affinity Ca^{2+} sensing, such as Asp-362/Asp-367 (30), Met-513 (31), and Glu-535 (32), and low affinity divalent cation sensing (Glu-374 and Glu-399) (30, 33–35). RCK2 encompasses a high affinity Ca^{2+}-binding site (the "calcium bowl") consisting of five consecutive Asp residues (Asp-894–Asp-898) (36–38) (Fig. 1*B*). Recently resolved crystal structures of this intracellular domain (27–29) provided details of its structural organization, consisting of four pairs of RCK domains that assemble into a tetrameric complex ("gating ring") akin to those of bacterial MthK channels (23) (Fig. 1*B*). Our recent work has shown that the purified BK gat-

* This work was supported, in whole or in part, by National Institutes of Health Grant R01GM082289 (to R. O.). This work was also supported by funds from the Laubisch Foundation (to R. O.) and American Heart Association Postdoctoral Fellowship (Western States Affiliate) 11POST7140046 (to A. P.).
[S] This article contains supplemental data and Figs. S1–S4.
[1] To whom correspondence should be addressed: Div. of Molecular Medicine, BH 570 CHS, Department of Anesthesiology, D. Geffen School of Medicine, University of California Los Angeles, CA 90075. Tel.: 310-206-2214; Fax: 310-206-1947; E-mail: rolcese@ucla.edu.

[2] The abbreviations used are: VSD, voltage-sensing domain; pWT, pseudo-WT; TMRM, tetramethylrhodamine-5′-maleimide.

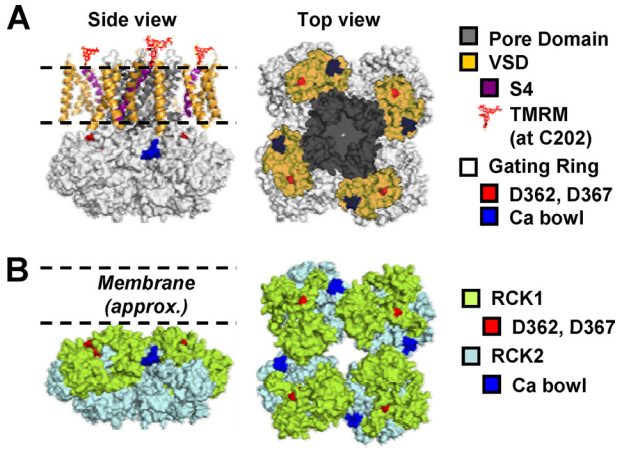

FIGURE 1. **BK channel putative structure and sensing domains.** *A, left panel*, side view of a putative structural model of the BK channel, composed of the BK gating ring structure (Protein Data Bank code 3NAF, *white*) (28), associated with the transmembrane portion of the $K_V1.2$–2.1 paddle chimera (Protein Data Bank code 2R9R) (67), and S0 ideal α helices positioned according to Liu *et al.* (68) as previously (51). The pore domain is shown in *gray*, whereas VSD helices are shown in *orange*, except S4 (*purple*). TMRM fluorophores conjugated with Cys-202 at the extracellular portions of S4 are shown in *red*. *Right panel*, top view of the gating ring structure overlaid by the "footprint" of the $K_V1.2$–2.1 transmembrane domains. *B*, side and top views of the human BK channel cytosolic gating ring apparatus (Protein Data Bank code 3NAF) (28) with its constituent domains RCK1 (*green*) and RCK2 (*light blue*). Asp-362 and Asp-367, which are involved in the RCK1 Ca^{2+} sensitivity, are shown in *red*. The calcium bowl (Asp-894–Asp-898) binding site in RCK2 is shown in *blue*. The approximate position of the phospholipid membrane is marked by the *dashed line*. Note that Asp-362/Asp-367 and the calcium bowl are potentially in close proximity to transmembrane voltage-sensing and pore domains.

ing ring selectively responds to Ca^{2+} and Mg^{2+} under physiologically relevant conditions, undergoing metal-driven conformational rearrangements, thus fulfilling its role as a chemomechanical transducer (39). Considering the highly allosteric nature of BK channel activation, these Ca^{2+}-induced conformational changes are expected to propagate to the transmembrane functional domains. In thermodynamic terms, the activation of Ca^{2+} sensors must alter the equilibrium isotherms of the pore and the VSD.

In the present work, we tested these premises and attempted to experimentally investigate whether the Ca^{2+}-induced conformational changes of the gating ring at the intracellular portion of the channel can propagate to, and be resolved as, structural rearrangements of the VSD. We combined the voltage-clamp fluorometry technique (40–42) with the UV photolysis of a Ca^{2+} cage compound, DM-Nitrophen (43–46), to simultaneously trigger voltage- and Ca^{2+}-dependent activations of BK channels. We found that rapid intracellular Ca^{2+} release produced structural rearrangements that not only increased channel P_o but also perturbed the conformation of the S4 helix of the BK VSD. In addition, impairing Ca^{2+} sensing in RCK2 (calcium bowl neutralization), but not in RCK1, abolished the effect of the elevation of intracellular Ca^{2+} concentration ($[Ca^{2+}]_i$) on VSD activation, underlining a functional difference of the two Ca^{2+} sensors. These findings were included in a statistical-mechanical allosteric model of BK channel activation, based on that by Horrigan and Aldrich (6) but expanded to take into account that the two high affinity Ca^{2+} sensors of the human BK channel are not functionally homologous. The fitting of experimental data to this new model allowed quantification of the distinct allosteric contribution of the two high affinity Ca^{2+}-sensing sites in the gating ring to VSD activation and pore opening, resolving the network of allosteric interactions underlying voltage- and Ca^{2+}-dependent BK channel activation.

EXPERIMENTAL PROCEDURES

Molecular Biology

The human *Slo1* clone (U11058) (47) without extracellular Cys (C14S/C141S/C277S) was used. Background mutations also included R207Q and W203V to increase P_o (17, 18) and fluorescence signal (20), respectively. A single Cys was substituted in position 202 in the short extracellular S3-S4 linker (S202C) for site-directed fluorescence labeling (19, 20, 48) (Fig. 1*A*). Throughout the paper, this clone is referred to as pseudo-WT (pWT). The two high affinity Ca^{2+} sensors were separately neutralized in the D362A/D367A (RCK1) and the D894N/D895N/D896N/D897N/D898N (RCK2/calcium bowl) mutants. We also used the noninactivating *Shaker* K^+ channel (Sh-IR, #M17211). For site-directed fluorescent labeling, we introduced a unique Cys in the S3-S4 linker (M356C) (40, 41). Single point mutations were generated with QuikChange site-directed mutagenesis kit (Stratagene, CA) and confirmed by sequencing. The cDNAs were translated to cRNAs *in vitro* (mMESSAGE MACHINE; Ambion, Austin, TX) and stored at −80 °C.

Oocyte Preparation

Xenopus laevis (NASCO, Modesto, CA) oocytes (stages V–VI) were prepared as previously described (49) and then injected with 50 nl of cRNA solution (0.01–0.1 μg/μl) using a Drummond nano-injector. The injected oocytes were maintained at 18 °C in an amphibian saline solution supplemented with 50 μg/ml gentamycin (Invitrogen), 200 μM DTT, and 10 μM EDTA. 3–6 days after injection, the oocytes were labeled with 10 μM membrane-impermeable, thiol-reactive fluorophore, tetramethylrhodamine-5′-maleimide (TMRM) (Molecular Probes, Eugene, OR) in a depolarizing K^+ solution (120 mM K-MES, 2 mM $Ca(MES)_2$, and 10 mM HEPES, pH 7). TMRM stock (100 mM) was dissolved in Me_2SO and stored at −20 °C. The oocytes were then thoroughly rinsed in a dye-free solution and injected with 100 nl of DM-Nitrophen precomplexed with Ca^{2+} (2.5 mM final concentration in the oocyte), prior to voltage clamp fluorometry.

Electrophysiological Techniques

Voltage Clamp Fluorometry—The cut open oocyte vaseline gap technique (50) is a low noise, fast clamp technique. Changes in fluorescence signal and ionic currents were simultaneously measured from the same area of membrane isolated by the top chamber (20, 42). The optical setup consists of a Zeiss Axioscope FS microscope with filters appropriate for TMRM (Omega Optical, Brattleboro, VT). The light source is a 100 W microscope halogen lamp. A TTL-triggered Uniblitz VS 25 shutter (Vincent Associates, Rochester, NY) is mounted on the excitation light path. The objective (Olympus LUMPlanFl, 40×, water immersion) has a numerical aperture of 0.8 and a

working distance of 3.3 mm (Olympus Optical). A Dagan Photomax 200 system is used for the amplification of the photocurrent and background fluorescence subtraction. A Xenon flash lamp system JML-C2 (Rapp Opto-electronik GmbH, Hamburg, Germany) delivering high energy UV flashes of adjustable intensity was used for the photolysis of caged Ca^{2+}. An external trigger synchronized UV flashes with voltage clamp and optical recordings. A water-immersed quartz light guide was positioned ~0.5 mm away from the oocyte upper dome.

Voltage Clamp Fluorometry Recording Solutions—The external solution contained 60 mM Na-MES, 50 mM K-MES, 2 mM $Ca(MES)_2$, 10 mM Na-HEPES (pH 7.0). The internal solution contained 120 mM potassium glutamate, 10 mM HEPES (pH 7.0). The solution for the intracellular pipette was 2700 mM Na-MES, 10 mM NaCl. Low access resistance to the oocyte interior was obtained by permeabilizing the oocyte with 0.1% saponin dissolved in the internal solution.

Analysis—The experimental data were analyzed with a customized program developed in our division and using fitting routines in Microsoft Excel. The data for the membrane conductance ($G(V)$) and the fluorescence ($F(V)$) curves were calculated from ionic current and fluorescence recordings, by averaging ~200 points (sampling frequency 50 μs/point) up to 2 ms before and 20 ms after Ca^{2+}-releasing UV flashes. The $G(V)$ curves were calculated by dividing the current-voltage relationships (I-V curves) by the driving force ($V_m - E_K$), where V_m is the membrane potential, and E_K is the equilibrium potential for K^+, estimated using the Nernst equation. $F(V)$ and $G(V)$ data points were fitted to one Boltzmann distribution of the following form,

$$G(V) = \frac{G_{max}}{1 + e^{\left[z(V_{half} - V_m)\left(\frac{F}{RT}\right)\right]}} \quad \text{(Eq. 1)}$$

$$F(V) = \frac{F_{max} - F_{min}}{1 + e^{\left[z(V_{half} - V_m)\left(\frac{F}{RT}\right)\right]}} - F_{min} \quad \text{(Eq. 2)}$$

where G_{max} and F_{max} are the maximal G and F; F_{min} is the minimal F; z is the effective valence of the distribution; V_{half} is the half-activating potential; V_m is the membrane potential; and F, R, and T are the usual thermodynamic values. The allosteric model is detailed in the supplemental data.

Patch Clamp—Membrane patches from *Xenopus* oocytes in the inside-out configuration were perfused with bath solutions containing 115 mM K-MES, 5 mM KCl, 5 mM HEDTA, 10 mM HEPES, pH 7 (supplemental Fig. S1*A*). $[Ca^{2+}]$ was varied by adding $CaCl_2$. The free $[Ca^{2+}]$ was theoretically calculated with WEBMAXC v2.10 and then measured using a Ca^{2+} electrode (WPI, Sarasota, FL). The borosilicate glass pipettes (WPI) were filled with the bath solution at the lowest free $[Ca^{2+}]$. The holding potential was 0 mV. The data were filtered to one-fifth of the sampling frequency. $G(V)$ curves for different BK clones (supplemental Fig. S1*B*) at different free $[Ca^{2+}]_i$ were constructed as described above. Plotting V_{half} against $[Ca^{2+}]$ produced calibration curves for the three BK clones used (supplemental Fig. S1*C*). To estimate the free $[Ca^{2+}]_i$ before and after UV photolysis in the voltage clamp fluorometry experiments, we used the relation between GV_{half} and free $[Ca^{2+}]$ in supplemental Fig. S1*C*.

Statistical Analysis

Scatter plots of ΔV_{half} *versus* $\Delta kT\ln[Ca^{2+}]_i$ were tested for monotonicity using Spearman's rank order correlation coefficient (ρ) using the statistical software SigmaStat (Aspire Software, Ashburn, VA). Analysis using Pearson's coefficient for linear dependence yielded similarly significant measures of correlation and therefore are not included. ΔV_{half} data were normalized to unitless quantities by multiplying by the fitted values for charge displacement (z_L for ΔGV_{half} and $4z_J$ for ΔFV_{half}) and dividing by the change in chemical potential for calcium $\Delta\mu = \Delta kT\ln[Ca^{2+}]_i$. The collective mean of these normalized quantities, which can be interpreted as a measure of thermodynamic linkage between Ca^{2+}- and voltage-sensing elements of the channel, was assessed for nonzero value using Student's t test. Of a total of 36 initially considered experiments, six were excluded either because: (i) $\Delta\mu$ did not exceed a post hoc threshold of 8 meV established to minimize error from insufficient calcium release (five experiments); or (ii) $[Ca^{2+}]_i$ was near the positive saturated range (~10^3 μM and higher), limiting the effect on ΔV_{half} (1 experiment). Including these experiments introduced outliers in the normalized data points but did not affect statistical outcomes.

RESULTS

Ca^{2+} Binding to BK Gating Ring Induces Structural Rearrangements in VSD—The human BK channel (Slo1) VSD has been studied using voltage clamp fluorometry and shown to undergo voltage-dependent molecular rearrangements (19, 20, 48, 51). In this work, BK channels were engineered to allow for specific fluorescent labeling of the extracellular side of the S4 transmembrane segment at position 202 (this BK construct is referred to as pseudo WT or pWT throughout this paper). As we have previously shown, TMRM labeling position 202 reports conformational changes related to BK VSD activation (19, 20, 48). Also, the TMRM fluorescence reported from the adjacent position 201 shares an almost identical voltage dependence with that of gating currents ($Q(V)$ curve) (20).

To probe for Ca^{2+}- induced conformational changes of the VSD, *Xenopus* oocytes expressing pWT BK (prelabeled with TMRM) were injected with DM-Nitrophen, a caged Ca^{2+} compound that undergoes UV photolysis, releasing Ca^{2+}. Thus, under voltage clamp (using the cut-open oocyte vaseline gap technique (50) modified for epifluorescence measurement (40–42)), we induced rapid increase of $[Ca^{2+}]_i$ by delivering UV flashes focused on the upper exposed oocyte membrane. Simultaneous recordings of K^+ currents and fluorescence emissions from an oocyte expressing pWT channels are shown in Fig. 2*A*. Ca^{2+} release was induced by UV flash triggered 60 ms after the onset of each depolarizing pulse. The rapid elevation of $[Ca^{2+}]_i$ increased the BK channel P_o, manifested by a downward or upward deflection of the ionic current traces (according to the K^+ reversal potential, −20 mV) (Fig. 2*A*, *black traces*). Notably, UV-induced Ca^{2+} uncaging also induced an increase of the simultaneously recorded TMRM fluorescence

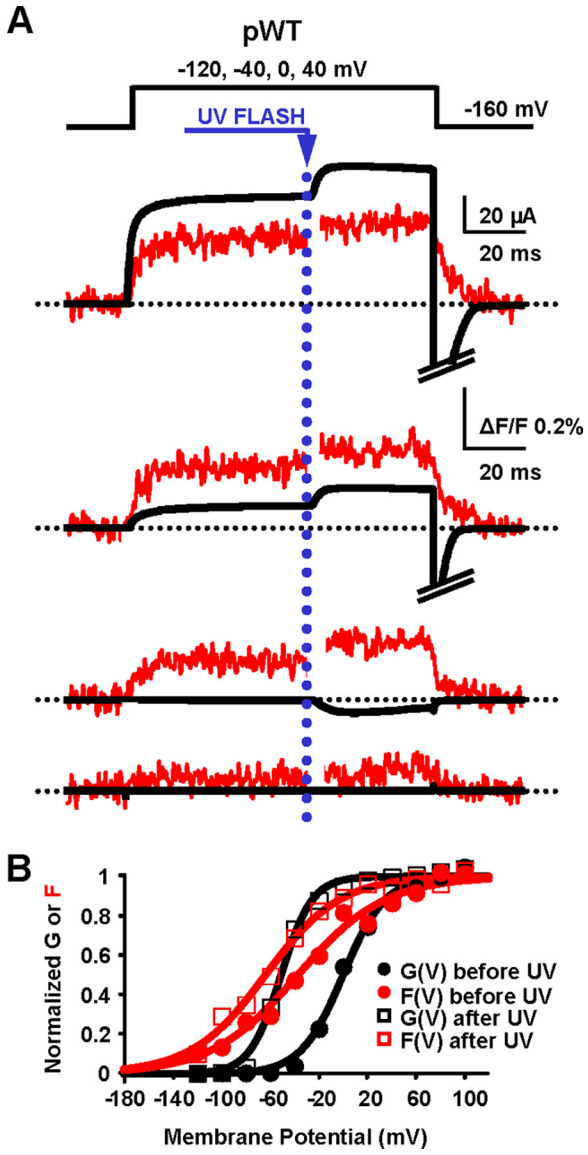

FIGURE 2. **Intracellular Ca^{2+} photo release induces conformational changes of the VSD of BK channels.** *A*, K^+ current and fluorescence traces simultaneously recorded during depolarizations to the indicated potentials from an oocyte expressing pWT channels are shown superimposed. Caged Ca^{2+} release was triggered 60 ms after the onset of depolarization by UV light flashes delivered onto the oocyte. In this experiment $[Ca^{2+}]_i$ increased from 10 to 84 μM. Ionic current and fluorescence signals increased following UV flashes. The photodiode amplifier was blanked for 3 ms during the UV flash to prevent overload. *B*, normalized fluorescence (*F*) and K^+ conductance (*G*) data from the experiment in *A*, before and after UV flashes, were fit to a single Boltzmann distribution. Both curves were leftward-shifted at high $[Ca^{2+}]_i$: before UV, $GV_{half} = 0$ mV and $FV_{half} = -37$ mV; after UV, $GV_{half} = -51$ mV and $FV_{half} = -63$ mV. Note the crossing of *G*(*V*) and *F*(*V*) curves after Ca^{2+} release, consistent with the view that Ca^{2+} can open BK channels at membrane potentials where VSDs are not activated (5, 6, 16, 52).

emission (Fig. 2*A*, *red traces*), suggesting that the Ca^{2+}-dependent activation of BK channels involves VSD conformational changes. The voltage dependence of the fluorescence deflections (*F*(*V*)) and macroscopic K^+ conductance (*G*(*V*)) were calculated from the fluorescence and ionic current recordings, 2 ms before and 20 ms after Ca^{2+}-releasing UV flashes (Fig. 2*B*). The rapid increase in $[Ca^{2+}]_i$ produced a hyperpolarizing shift of the *G*(*V*) curve ($\Delta GV_{half} \approx -50$ mV) associated with a smaller, but well resolved, translation of the *F*(*V*) curve in the same direction ($\Delta FV_{half} \approx -25$ mV). Note that the Ca^{2+} release induced a crossover of *G*(*V*) and *F*(*V*) curves (Fig. 2*B*), evidence for BK channels undergoing conformational transitions while in the open state (5, 6, 16, 52).

The effects observed in BK channels were genuinely produced by Ca^{2+}, as confirmed by the lack of detectable changes in ionic current and fluorescence recordings when Ca^{2+}-insensitive Shaker K^+ channels, fluorescently labeled to resolve their S4 movements, were similarly subjected to UV-induced Ca^{2+} release (supplemental Fig. S2, *A* and *B*). Moreover, ionic current and fluorescence recordings from pWT BK channels expressed in oocytes not injected with DM-Nitrophen were unaffected by UV flashes (supplemental Fig. S2, *C* and *D*). The reproducibility of Ca^{2+} photo release during sequential pulses is demonstrated in supplemental Fig. S3, *A* and *B*, which also shows that $[Ca^{2+}]_i$ returned to its basal level in less than 1 s (supplemental Fig. S3*C*).

To estimate the local intracellular free $[Ca^{2+}]_i$ before and after UV photolysis, we exploited the BK intrinsic Ca^{2+} sensing properties (*i.e.* the dependence of the half activation potential GV_{half} on $[Ca^{2+}]_i$), as previously utilized in motor neurons and hair cells (53, 54). GV_{half} *versus* free $[Ca^{2+}]$ calibration curves were constructed from excised patch experiments (see "Experimental Procedures" and supplemental Fig. S1). Note that in the pWT background, Ca^{2+} sensitivity was reduced by the well documented mutations in RCK1 and RCK2 domains, recapitulating the effect observed in WT BK channels (30, 36).

The Calcium Bowl Is Required for Ca^{2+}-mediated Effect on VSD Movements—Two high affinity Ca^{2+}-sensing sites are located within the BK gating ring ligand binding apparatus: one, in the RCK2 domain, coordinates Ca^{2+} via the five Asp residues (Asp-894–Asp-898) comprising the calcium bowl (27, 29, 36); the other, in RCK1, includes residue Asp-367, which is critical for Ca^{2+} sensing (30) (its Ca^{2+}-coordinating role has been suggested (32) but not yet experimentally demonstrated (25, 27, 29)). These Ca^{2+}-sensing sites differ in several respects, including: structure and relative positions within the gating ring and RCK domains (Fig. 1) (27–29); affinity and selectivity for divalent cations (34); apparent voltage dependence of Ca^{2+} binding (55); and role in epilepsy/dyskinesia-causing BK channel mutants (56). Given these established differences, we asked whether the two high affinity Ca^{2+} sensors also exert different contributions to the pore and VSD activation. To assess the role of these modules in the allosteric interaction between the gating ring and the VSD, the two high affinity Ca^{2+}-sensing sites were separately neutralized by introducing mutations D362A/D367A (in RCK1) (30) and D894N/D895N/D896N/D897N/D898N (in RCK2) (36). In individual experiments measuring D362A/D367A channels, following UV flash photolysis, the rapid increase of $[Ca^{2+}]_i$ induced a detectable shift toward more negative potentials in both the *G*(*V*) and *F*(*V*) curves. The shift was in the same direction as was observed in pWT channels, but smaller (Fig. 3, *A* and *B*), suggesting that residues Asp-362/Asp-367 are not necessary to mediate the propagation of Ca^{2+}-induced gating ring rearrangements to the VSD.

On the other hand, in D894N/D895N/D896N/D897N/D898N channels, there was no obvious effect of intracellular Ca^{2+} release on the *F*(*V*) curve (Fig. 3, *C* and *D*). Still, the P_o of

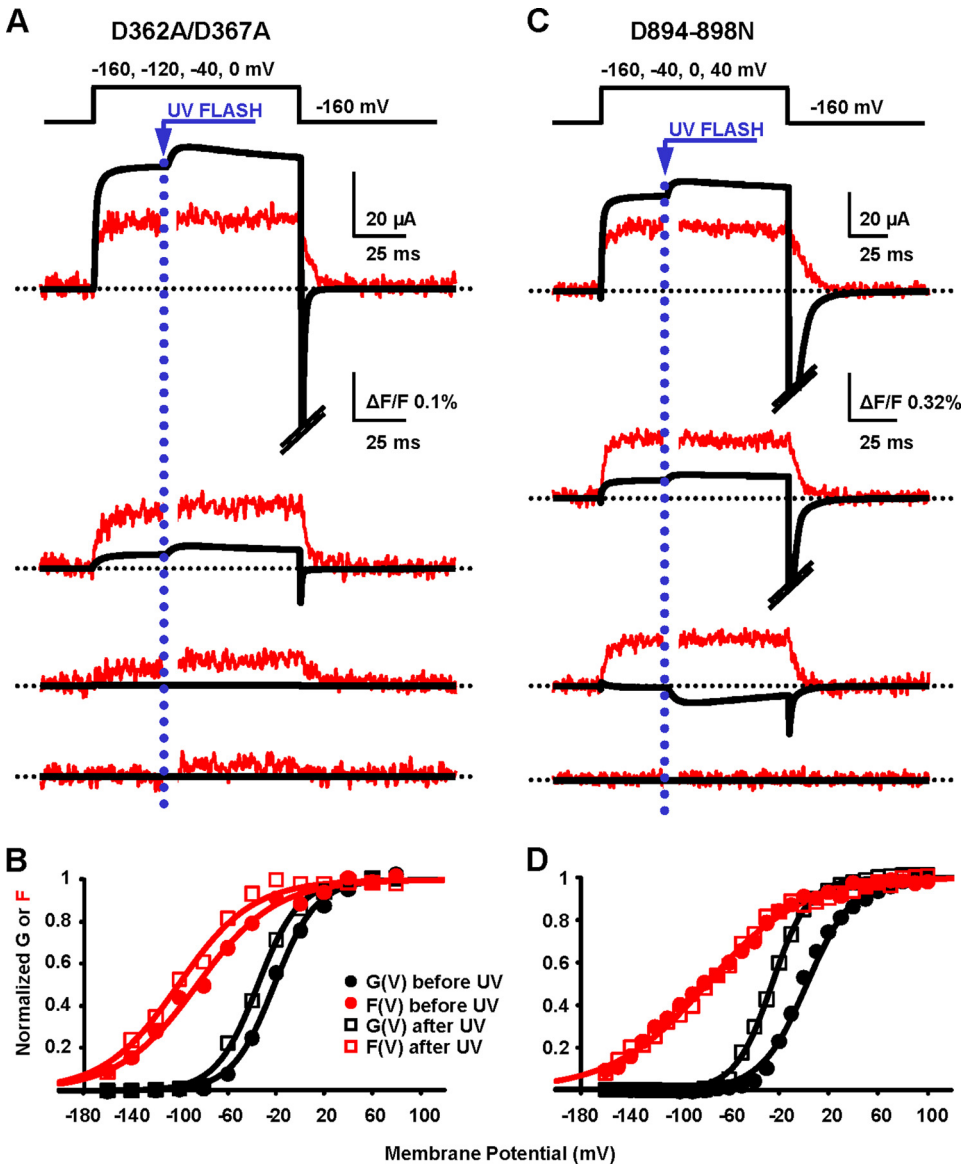

FIGURE 3. **RCK1 and RCK2 are not functionally equivalent Ca^{2+} sensors.** *A*, K^+ current and fluorescence traces simultaneously recorded during depolarizations to the indicated potentials from a representative oocyte expressing BK channels with neutralized high affinity Ca^{2+} sensing in RCK1 (D362A/D367A) are shown superimposed. Caged Ca^{2+} release was triggered 35 ms after the onset of depolarization by challenging the oocyte with UV light to produce $[Ca^{2+}]_i$ increase from 137 to 320 μM. As in the pWT channels, ionic current and fluorescence increased following UV flash. The photodiode amplifier was blanked for 3 ms during the UV flash to prevent overload. *B*, normalized fluorescence (*F*) and K^+ conductance (*G*) data from the experiment in *A*, before and after UV flashes, were fit to a single Boltzmann distribution. Both curves were leftward-shifted at high $[Ca^{2+}]_i$: before UV, $GV_{half} = -21$ mV and $FV_{half} = -85$ mV; after UV, $GV_{half} = -35$ mV and $FV_{half} = -101$ mV. *C*, as in *A*, from an oocyte expressing BK channels with neutralized calcium bowl in RCK2 (D894N/D895N/D896N/D897N/D898N, *D894–898N*). Following UV flash, $[Ca^{2+}]_i$ increased from 105 to 210 μM. Only ionic currents were affected by Ca^{2+} uncaging. *D*, as in *B*, for data from calcium bowl mutant in *C*. Before UV, $GV_{half} = 3$ mV and $FV_{half} = -79$ mV; after UV, $GV_{half} = -26$ mV and $FV_{half} = -78$ mV.

this mutant was increased by the elevation of $[Ca^{2+}]_i$, as demonstrated by the leftward-shifted $G(V)$ curve following Ca^{2+} release (Fig. 3*D*). The absence of detectable Ca^{2+}-induced VSD conformational changes excludes a direct effect of Ca^{2+} on the BK VSD (*e.g.*, mediated by a charge screening effect), implying a functional, allosteric coupling between the calcium bowl and VSD.

We analyzed results from all experiments, as depicted in Fig. 4. The Ca^{2+}-induced shift of the half-activation potential of $G(V)$ curves (ΔGV_{half}) was consistently associated with a shift of the $F(V)$ curves (ΔFV_{half}) in the same direction, but only with an intact calcium bowl (Fig. 4*A*). To quantify the dependence of observed shifts in $G(V)$ and $F(V)$ curves upon Ca^{2+} release in pWT and mutants channels, we performed a statistical analysis as described under "Experimental Procedures." We found a strong monotonic correlation between Ca^{2+} release ($\Delta kT\ln[Ca^{2+}]$) and $G(V)$ and $F(V)$ voltage shifts in pWT and in the D362A/D367A mutant (Fig. 4, *B* and *C*). This was also true for the D894N/D895N/D896N/D897N/D898N mutant in the case of $z_L{}^*GV_{half}$ ($p < 0.001$), but not in the case of $4z_J{}^*\Delta F - V_{half}$ ($p = 0.705$). Furthermore, normalizing the voltage shifts by the change in Ca^{2+} chemical potential ($\Delta\mu$) abolished the correlation between shifts of FV_{half} and GV_{half} as shown by theclustering of the data points (Fig. 4, *E–G*). We interpreted these data as a demonstration of the obligatory dependence of FV_{half} and GV_{half} on $[Ca^{2+}]$. The normalized voltage shift

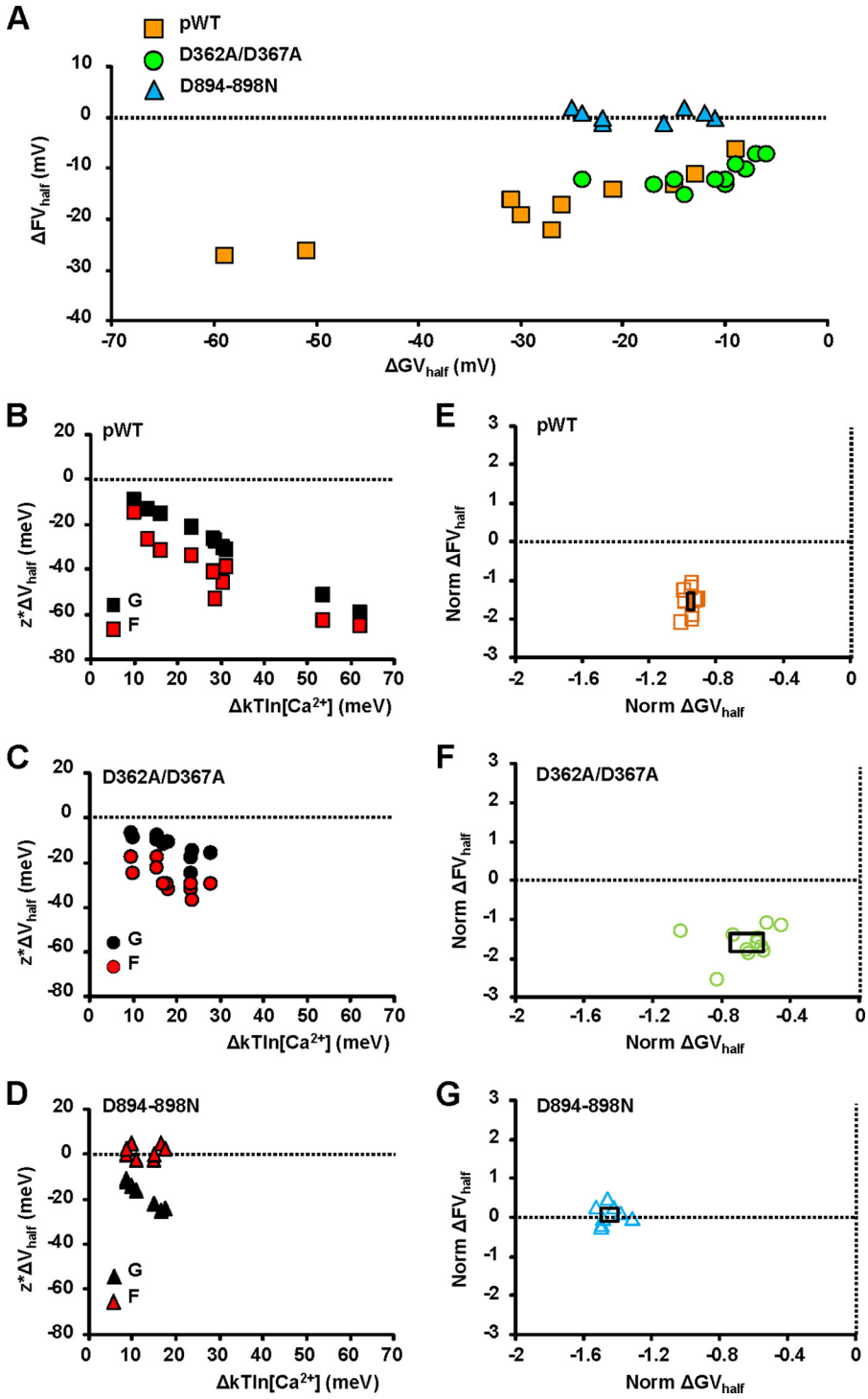

FIGURE 4. **Compilation of experiments measuring shifts in GV_{half} and FV_{half} in response to calcium release: an intact calcium bowl is necessary to mediate the allosteric interaction between the VSD and the gating ring.** *A*, scatter plot of ΔFV_{half} *versus* ΔGV_{half} for all experiments meeting inclusion criteria described under "Experimental Procedures." *B–D*, changes in activation energy produced by UV-flash triggered release (z_L*ΔGV_{half} and $4z_J$*ΔFV_{half}) plotted against $\Delta kT\ln[Ca]$. A strong monotonic correlation exists between calcium release and *G*(*V*) and *F*(*V*) voltage shifts in pWT BK (z_L*GV_{half}: $\rho = -1.0$, $p < 0.001$; $4z_J$*FV_{half}: $\rho = -0.915$, $p < 0.001$) and in the D362A/D367A mutant (z_L*GV_{half}: $\rho = -0.868$, $p < 0.001$; $4z_J$*FV_{half}: $\rho = -0.787$, $p = 0.002$). This is also true for the D894N/D895N/D896N/D897N/D898N (*D894–898N*) mutant in the case of z_L*ΔGV_{half} ($\rho = -0.970$, $p < 0.001$), but not in the case of $4z_J$*ΔFV_{half} ($\rho = 0.146$, $p = 0.705$). *E–G*, normalizing the voltage shifts by dividing by the change in calcium chemical potential eliminated the correlation between ΔFV_{half} and ΔGV_{half} (pWT: $\rho = 0.079$, $p = 0.811$; D362A/D367A: $\rho = 0.336$, $p = 0.296$; D894N/D895N/D896N/D897N/D898N: $\rho = 0.144$, $p = 0.705$). The *rectangles* superimposed onto the scatter points indicate the 95% confidence interval for the mean value in both axes. The only case where the normalized voltage shift was not statistically different from zero was for D894N/D895N/D896N/D897N/D898N ΔFV_{half} ($p = 0.27$; otherwise $p < 0.001$).

was statistically different from zero for all channels in the case of *G*(*V*) and also for pWT and RCK1 mutant D362A/D367A in the case of *F*(*V*) (Fig. 4, *E* and *F*), but there was no significantly detectable shift in $4z_J$*$\Delta FV_{half}/\Delta\mu$ in the case of RCK2 mutant D894N/D895N/D896N/D897N/D898N (Fig. 4*G*). Thus, with the exception of the RCK2 mutant, an

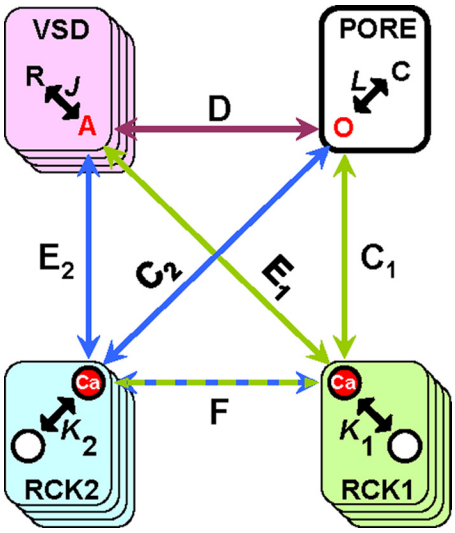

FIGURE 5. **An allosteric model of BK channel activation.** The schematic representation of the model includes a pore domain and three regulatory domains: the VSD and two Ca^{2+}-sensing domains (RCK1 and RCK2) per subunit. Intrinsic gating between closed (*C*) and open (*O*) states of the pore domain is specified by the voltage-dependent equilibrium constant *L*; the VSD can be found either in the resting (*R*) or active (*A*) state according to equilibrium constant *J*; Ca^{2+} sensors can exist in unbound or Ca^{2+}-bound states according to equilibrium constants K_1 and K_2. *D*, C_1, C_2, E_1, E_2, and *F* are allosteric factors (see supplemental data).

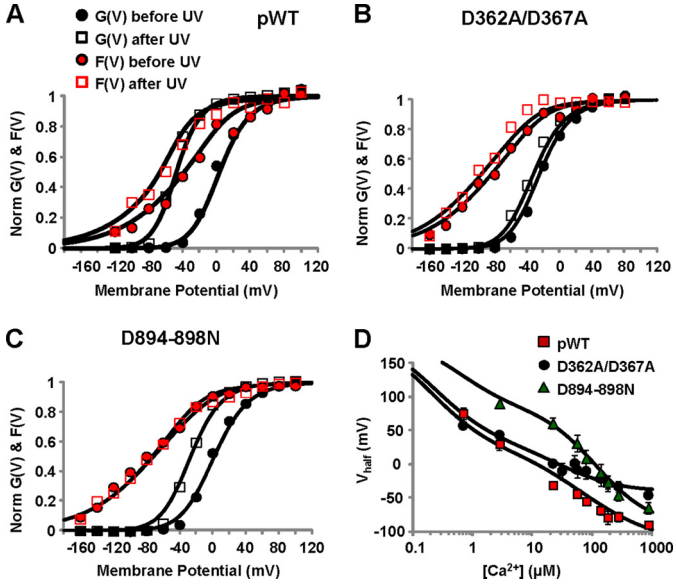

FIGURE 6. **The allosteric model for BK channel activation fits experimental data from three different BK channel mutants.** The experimental GV and FV data for pWT (*A*), RCK1 mutant D362A/D367A (*B*), and RCK2 mutant D894N/D895N/D896N/D897N/D898N (*D894–898N*, *C*) were fitted simultaneously together with the data points describing the Ca^{2+} dependence of the GV_{half} (*D*). The *continuous lines* are the predictions of the BK allosteric model presented in Fig. 5 (experimental data are as in Figs. 2 and 3, and supplemental Fig. S1*C*). The fitted parameters are listed in Table 1.

increase in intracellular $[Ca^{2+}]$ consistently produced a leftward shift in the activation curves (ΔGV_{half}) associated with a statistically significant shift of the voltage sensor activation (ΔFV_{half}) in the same direction.

These results suggest that RCK1 and RCK2 employ different allosteric pathways to bring about Ca^{2+}-mediated activation. To quantify the mechanistic interpretation of the experimental results, we fit the data with an allosteric statistical-mechanical model.

An Allosteric Model of BK Channel That Accounts for Presence of Two High Affinity Ca^{2+} Sensors per Subunit—The experimental data suggest that Ca^{2+} binding to RCK1 and RCK2 high affinity Ca^{2+} sensors results in different effects on BK activation. To interpret our data in the context of an allosteric scheme, we constructed a statistical-mechanical model inspired by the equilibrium Horrigan and Aldrich model of BK channel activation (6). The Horrigan and Aldrich model describes the allosteric interactions linking voltage sensing, Ca^{2+} binding, and pore opening in BK channels. We expanded on the Horrigan and Aldrich model to include two Ca^{2+}-sensing domains per subunit (Fig. 5 and supplemental data), each capable of interacting with the Pore (allosteric factors C_1 and C_2), with the VSD (allosteric factors E_1 and E_2), and with each other (allosteric factor *F*). The normalized $G(V)$ and $F(V)$ data obtained at two different $[Ca^{2+}]$ (before and after UV photolysis) from pWT, RCK1 mutant, and RCK2 mutant channels were simultaneously fit to the model (Fig. 6 and Table 1): $F(V)$ data were fit to the model prediction of VSD activation, whereas $G(V)$ data were fit with P_o, as previously (19). As a further constraint, we simultaneously fit averaged values of GV_{half} as a function of $[Ca^{2+}]$ for the three BK channel clones (supplemental Fig. S1*C* and Fig. 6*D*). In fitting the mutant channels, we minimized the number of parameters needed to obtain good

TABLE 1

Fitting parameters for the model predictions shown in Fig. 6

For the mutants only parameters different from pWT are reported.

Domain or Interaction	Parameters	Ca^{2+}-sensing mutations		
		pWT	D362/367A	D894N/D895N/D896N/D897N/D898N
Pore	z_L (e^0)	1.00		
	V_L (mV)	307		
S4	z_J (e^0)	0.60		
	V_J (mV)	20		
RCK1	K_{d1} (μM)	10.03		
RCK2	K_{d2} (μM)	2.98		4820
S4-Pore	*D*	3.34		
RCK1-Pore	C_1	2.84	1.00	
RCK1-S4	E_1	10.00		
RCK2-Pore	C_2	10.41		
RCK2-S4	E_2	2.28		0.70
RCK1-RCK2	*F*	0.02	0.06	11.60

fits while constraining the remaining variables to their pWT equivalent. Because it appears that RCK1 retains its high affinity Ca^{2+} binding properties when D362/D367 are neutralized (25), K_{d1} in the RCK1 mutant was constrained to be equal to the corresponding pWT value. Intersubunit interactions between BK regulatory domains were forbidden; previous work has indicated that such interactions do not play a major role (57).

The best set of fitting parameters that accounts for the experimental data is reported in Table 1. The valence of the VSD charge is $z_J = 0.6\ e^0$, similar to what has been reported for the R207Q BK channel (18). The opening of the channel (C–O transition) is also intrinsically voltage-dependent ($z_L = 1\ e^0$), in general agreement with previous works (6, 18). During the simultaneous fitting, the intrinsic Ca^{2+} dissociation constants for RCK1 (K_{d1}) and RCK2 (K_{d2}) were constrained to within the range reported by a recent study (55), resulting in $K_{d1} = 10.03$ μM and $K_{d2} = 2.98$ μM for pWT channels (Fig. 6*A*). We also

found that, in the Ca^{2+}-bound state, RCK1 strongly stabilized VSD activation ($E_1 = 10$) and, to a lesser extent, the conducting state ($C_1 = 2.84$). On the other hand, RCK2 efficiently facilitated pore operation ($C_2 = 10.41$) and exerted a positive cooperativity on VSD activation ($E_2 = 2.28$). A negative cooperativity was exhibited between the two Ca^{2+}-sensing domains ($F = 0.02$), as also suggested by a previous investigation (55).

In the RCK1 mutant channels (Fig. 6*B* and Table 1), D362A/D367A mutations abolished the RCK1-Pore cooperativity ($C_1 = 1$) and slightly affected the allosteric factor F (from 0.02 to 0.06), leaving unaltered the RCK1-VSD interaction. In agreement with the consolidated knowledge that the neutralization of the calcium bowl (D894N/D895N/D896N/D897N/D898N) impairs high affinity Ca^{2+} sensing (36) by reducing Ca^{2+} binding affinity (24, 37, 38, 58), the model predicted a marked increase in K_{d2} in the D894N/D895N/D896N/D897N/D898N mutant ($K_{d2} = 4820\ \mu M$) (Fig. 6*C* and Table 1). The allosteric interaction RCK2-Pore (C_2) did not vary compared with the pWT channel. Instead, a negative cooperativity was found between RCK2 and VSD ($E_2 = 0.7$). In addition, RCK1-RCK2 interaction becomes stronger ($F = 11.6$).

DISCUSSION

BK channels combine properties of both voltage- and ligand-gated ion channels, a feature that allows them to integrate information on membrane potential and $[Ca^{2+}]_i$ to control key physiological processes such as the smooth muscle tone, cochlear hair cell tuning, neuronal excitability, neurotransmitter release, insulin secretion, and oxygen sensing (10, 11, 59–63). The interaction between voltage and Ca^{2+} sensing mechanisms was proposed for native BK channels reconstituted in lipid bilayer (52) and further investigated in cloned BK channels, demonstrating the allosteric nature of the dual activation mechanism (6, 9, 12, 55, 64). In this work, the interplay between transmembrane VSD and intracellular gating ring with the BK pore was investigated using voltage-clamp fluorometry combined with UV flash photolysis of DM-Nitrophen to elicit a fast, reversible, and reproducible increase in intracellular free $[Ca^{2+}]$ (Fig. 2 and supplemental Figs. S2 and S3). In the human BK channel (Slo1), we provided experimental evidence that the rapid increase of $[Ca^{2+}]_i$ induces a conformational change that, originating in the gating ring, propagates to the VSD, facilitating its activation (Figs. 2*A* and 4). Indeed, the purified BK gating ring in solution can undergo Ca^{2+}-driven structural rearrangements, resulting in an overall decrease of its hydrodynamic radius (39). Likely, both RCK1 and RCK2 contribute to the Ca^{2+}-induced rearrangements of the gating ring, based on the sensor/transducer properties of isolated RCK1 and RCK2 homomers (24, 25).

Moreover, a physical proximity of VSD and gating ring is suggested by their mutual coordination of Mg^{2+} (10, 11, 35, 65). Atomic structures of the BK gating ring (27–29), have pinpointed the locations of the calcium bowl (in RCK2) and Asp-362/Asp-367 residues (in RCK1) that, in the whole channel, could face the intracellular portion of the VSD (Fig. 1).

Using a statistical-mechanical model inspired by the Horrigan and Aldrich model (6) but accounting for two distinct Ca^{2+} sensors (Fig. 5), we quantified the allosteric interactions between pore, VSD, and the two RCK domains. In pWT channels, the model predicted salient differences in the allosteric coupling between RCK1 and RCK2 with the VSD and the pore (Table 1), suggesting that they are functionally separable, despite their structural homology. RCK1 and RCK2 are allosterically coupled by negative cooperativity, such that the activation of one domain disfavors the activation of the other, recapitulating the findings of Sweet and Cox (55). The functional impairment of Ca^{2+} sensing either in RCK1 or in RCK2 highlighted their functional diversity. In D362A/D367A mutants, a rapid increase in $[Ca^{2+}]_i$ significantly facilitated pore and VSD activation (Figs. 3*A* and *4*), as indicated by the consistent leftward shifts of both $G(V)$ and $F(V)$ curves at the highest $[Ca^{2+}]_i$ (Figs. 3*B* and 4). This effect was likely mediated by intact calcium bowls in RCK2 domains. The effect of the D362A/D367A is largely accounted for by the loss of cooperativity between RCK1 and the pore (allosteric factor C_1) (Table 1 and Fig. 6*B*). It is interesting that the model can account for the effects of the D362A/D367A mutation without reducing the intrinsic Ca^{2+} affinity of the RCK1 domain (K_{d1}). This prediction would be in agreement with the lack of direct experimental evidence that Asp-362/Asp-367 residues are essential for Ca^{2+} coordination. However, a potential Ca^{2+}-binding site involving Asp-367 and other residues has been proposed based on electrophysiological evidence (30, 34, 55) and inference from the gating ring crystal structure (28, 32). Interestingly, the neutralization of calcium bowl abolished the Ca^{2+}-induced facilitation of the VSD activation; indeed, the $F(V)$ curves were not significantly modified by the Ca^{2+} release (Figs. 3*D* and 4). To account for these experimental data, three model parameters were considerably altered compared with the corresponding pWT values (Table 1), suggesting that the neutralization of the five Asp residues not only abolished a high affinity Ca^{2+}-binding site (calcium bowl) but also altered the energetics of gating ring operation, likely because of a structural perturbation.

Recent work has pointed out an important functional difference between RCK1 and RCK2: Ca^{2+} binding to the RCK1 domain (but not to RCK2) is voltage-dependent (55). To test the validity of our model prediction, we computed the steady-state occupancy of the Ca^{2+}-bound state for RCK1 and RCK2. We found that, for a wide range of membrane potentials, the occupancy of RCK1 Ca^{2+}-bound state was voltage-dependent, whereas RCK2 Ca^{2+} binding was weakly affected by membrane potential (supplemental Fig. S4). Thus, despite their structural homology, RCK1 and RCK2 domains provide different contribution to the Ca^{2+}-dependent activation of BK channels.

The importance of achieving a deeper understanding of the BK channel biophysical properties resides in its involvement in several diseases, such as hypertension, epilepsy, schizophrenia, and diabetes (11, 62, 63, 66). In particular, elucidating the mechanisms underlying the functional coupling between VSD and the two distinct Ca^{2+} sensors is fundamental for the physiology and pathophysiology of excitable cells. For instance, the Slo1 epilepsy/dyskinesia-causing mutation affects Ca^{2+}-dependent activation originating from the Ca^{2+}-binding site in RCK1, but not in RCK2, by altering the coupling mechanism between Ca^{2+} binding and gate opening (56).

In summary, we have directly probed the allosteric nature of BK channel Ca^{2+}-dependent activation by optically tracking VSD movements perturbed by Ca^{2+} binding to the gating ring, under voltage clamp. By investigating channels impaired in high affinity Ca^{2+}-sensing sites, we revealed that the two BK Ca^{2+} sensors are not functionally equivalent: although both contribute to Ca^{2+}-dependent channel activation, the efficiency of the allosteric interactions appears different. A functional calcium bowl (RCK2) is required to observe the propagation of Ca^{2+}-induced "wave" of rearrangements from the cytoplasmic portion to the transmembrane VSD. The results were fit with a statistical-mechanical allosteric model to quantify the cooperative interactions among the prominent BK regulatory domains. Although this approach was successful in dissecting the allosteric contributions of high affinity Ca^{2+}-sensing domains to BK channel activation, it did not explore the role of low affinity Ca^{2+}-sensing sites (30, 33–35), because the experimental [Ca^{2+}] range was limited to prevent their significant engagement. Nevertheless, it would be of great interest to further investigate their allosteric contribution to BK channel operation to better understand the complex mechanism of BK channel activation.

Acknowledgment—The Slo1 clone was a kind gift from Ligia Toro.

REFERENCES

1. del Sol, A., Tsai, C. J., Ma, B., and Nussinov, R. (2009) The origin of allosteric functional modulation. Multiple pre-existing pathways. *Structure* **17,** 1042–1050
2. Goodey, N. M., and Benkovic, S. J. (2008) Allosteric regulation and catalysis emerge via a common route. *Nat. Chem. Biol.* **4,** 474–482
3. Piper, D. R., Rupp, J., Sachse, F. B., Sanguinetti, M. C., and Tristani-Firouzi, M. (2008) Cooperative interactions between R531 and acidic residues in the voltage sensing module of hERG1 channels. *Cell Physiol. Biochem.* **21,** 37–46
4. Zandany, N., Ovadia, M., Orr, I., and Yifrach, O. (2008) Direct analysis of cooperativity in multisubunit allosteric proteins. *Proc. Natl. Acad. Sci. U.S.A.* **105,** 11697–11702
5. Magleby, K. L. (2003) Gating mechanism of BK (Slo1) channels. So near, yet so far. *J. Gen. Physiol.* **121,** 81–96
6. Horrigan, F. T., and Aldrich, R. W. (2002) Coupling between voltage sensor activation, Ca^{2+} binding and channel opening in large conductance (BK) potassium channels. *J. Gen. Physiol.* **120,** 267–305
7. Taraska, J. W., and Zagotta, W. N. (2007) Structural dynamics in the gating ring of cyclic nucleotide-gated ion channels. *Nat. Struct. Mol. Biol.* **14,** 854–860
8. Altomare, C., Bucchi, A., Camatini, E., Baruscotti, M., Viscomi, C., Moroni, A., and DiFrancesco, D. (2001) Integrated allosteric model of voltage gating of HCN channels. *J. Gen. Physiol.* **117,** 519–532
9. Latorre, R., Morera, F. J., and Zaelzer, C. (2010) Allosteric interactions and the modular nature of the voltage- and Ca^{2+}-activated (BK) channel. *J. Physiol.* **588,** 3141–3148
10. Hou, S., Heinemann, S. H., and Hoshi, T. (2009) Modulation of BKCa channel gating by endogenous signaling molecules. *Physiology* **24,** 26–35
11. Lee, U. S., and Cui, J. (2010) BK channel activation. Structural and functional insights. *Trends Neurosci.* **33,** 415–423
12. Rothberg, B. S., and Magleby, K. L. (2000) Voltage and Ca^{2+} activation of single large-conductance Ca^{2+}-activated K^+ channels described by a two-tiered allosteric gating mechanism. *J. Gen. Physiol.* **116,** 75–99
13. Shen, K. Z., Lagrutta, A., Davies, N. W., Standen, N. B., Adelman, J. P., and North, R. A. (1994) Tetraethylammonium block of Slowpoke calcium-activated potassium channels expressed in *Xenopus* oocytes. Evidence for tetrameric channel formation. *Pflugers Arch.* **426,** 440–445
14. Wallner, M., Meera, P., and Toro, L. (1996) Determinant for β-subunit regulation in high-conductance voltage-activated and Ca^{2+}-sensitive K+ channels. An additional transmembrane region at the N terminus. *Proc. Natl. Acad. Sci. U.S.A.* **93,** 14922–14927
15. Armstrong, C. M. (2003) Voltage-gated K channels. *Sci. STKE.* **2003,** re10
16. Stefani, E., Ottolia, M., Noceti, F., Olcese, R., Wallner, M., Latorre, R., and Toro, L. (1997) Voltage-controlled gating in a large conductance Ca^{2+}-sensitive K+ channel (hslo). *Proc. Natl. Acad. Sci. U.S.A.* **94,** 5427–5431
17. Díaz, L., Meera, P., Amigo, J., Stefani, E., Alvarez, O., Toro, L., and Latorre, R. (1998) Role of the S4 segment in a voltage-dependent calcium-sensitive potassium (hSlo) channel. *J. Biol. Chem.* **273,** 32430–32436
18. Ma, Z., Lou, X. J., and Horrigan, F. T. (2006) Role of charged residues in the S1–S4 voltage sensor of BK channels. *J. Gen. Physiol.* **127,** 309–328
19. Pantazis, A., Gudzenko, V., Savalli, N., Sigg, D., and Olcese, R. (2010) Operation of the voltage sensor of a human voltage- and Ca^{2+}-activated K^+ channel. *Proc. Natl. Acad. Sci. U.S.A.* **107,** 4459–4464
20. Savalli, N., Kondratiev, A., Toro, L., and Olcese, R. (2006) Voltage-dependent conformational changes in human Ca^{2+}- and voltage-activated K^+ channel, revealed by voltage-clamp fluorometry. *Proc. Natl. Acad. Sci. U.S.A.* **103,** 12619–12624
21. Lu, R., Alioua, A., Kumar, Y., Eghbali, M., Stefani, E., and Toro, L. (2006) MaxiK channel partners. Physiological impact. *J. Physiol.* **570,** 65–72
22. Jiang, Y., Pico, A., Cadene, M., Chait, B. T., and MacKinnon, R. (2001) Structure of the RCK domain from the *E. coli* K^+ channel and demonstration of its presence in the human BK channel. *Neuron* **29,** 593–601
23. Jiang, Y., Lee, A., Chen, J., Cadene, M., Chait, B. T., and MacKinnon, R. (2002) Crystal structure and mechanism of a calcium-gated potassium channel. *Nature* **417,** 515–522
24. Yusifov, T., Savalli, N., Gandhi, C. S., Ottolia, M., and Olcese, R. (2008) The RCK2 domain of the human BKCa channel is a calcium sensor. *Proc. Natl. Acad. Sci. U.S.A.* **105,** 376–381
25. Yusifov, T., Javaherian, A. D., Pantazis, A., Gandhi, C. S., and Olcese, R. (2010) The RCK1 domain of the human BKCa channel transduces Ca^{2+} binding into structural rearrangements. *J. Gen. Physiol.* **136,** 189–202
26. Roosild, T. P., Lê, K. T., and Choe, S. (2004) Cytoplasmic gatekeepers of K^+-channel flux. A structural perspective. *Trends Biochem. Sci.* **29,** 39–45
27. Yuan, P., Leonetti, M. D., Pico, A. R., Hsiung, Y., and MacKinnon, R. (2010) Structure of the human BK channel Ca^{2+}-activation apparatus at 3.0 A resolution. *Science* **329,** 182–186
28. Wu, Y., Yang, Y., Ye, S., and Jiang, Y. (2010) Structure of the gating ring from the human large-conductance Ca^{2+}-gated K^+ channel. *Nature* **466,** 393–397
29. Yuan, P., Leonetti, M. D., Hsiung, Y., and MacKinnon, R. (2012) Open structure of the Ca^{2+} gating ring in the high-conductance Ca^{2+}-activated K^+ channel. *Nature* **481,** 94–97
30. Xia, X. M., Zeng, X., and Lingle, C. J. (2002) Multiple regulatory sites in large-conductance calcium-activated potassium channels. *Nature* **418,** 880–884
31. Bao, L., Rapin, A. M., Holmstrand, E. C., and Cox, D. H. (2002) Elimination of the BK(Ca) channel's high-affinity Ca^{2+} sensitivity. *J. Gen. Physiol.* **120,** 173–189
32. Zhang, G., Huang, S. Y., Yang, J., Shi, J., Yang, X., Moller, A., Zou, X., and Cui, J. (2010) Ion sensing in the RCK1 domain of BK channels. *Proc. Natl. Acad. Sci. U.S.A.* **107,** 18700–18705
33. Shi, J., Krishnamoorthy, G., Yang, Y., Hu, L., Chaturvedi, N., Harilal, D., Qin, J., and Cui, J. (2002) Mechanism of magnesium activation of calcium-activated potassium channels. *Nature* **418,** 876–880
34. Zeng, X. H., Xia, X. M., and Lingle, C. J. (2005) Divalent cation sensitivity of BK channel activation supports the existence of three distinct binding sites. *J. Gen. Physiol.* **125,** 273–286
35. Yang, H., Shi, J., Zhang, G., Yang, J., Delaloye, K., and Cui, J. (2008) Activation of Slo1 BK channels by Mg^{2+} coordinated between the voltage sensor and RCK1 domains. *Nat. Struct. Mol. Biol.* **15,** 1152–1159
36. Schreiber, M., and Salkoff, L. (1997) A novel calcium-sensing domain in the BK channel. *Biophys. J.* **73,** 1355–1363
37. Bian, S., Favre, I., and Moczydlowski, E. (2001) Ca^{2+}-binding activity of a COOH-terminal fragment of the *Drosophila* BK channel involved in Ca^{2+}-dependent activation. *Proc. Natl. Acad. Sci. U.S.A.* **98,** 4776–4781

38. Bao, L., Kaldany, C., Holmstrand, E. C., and Cox, D. H. (2004) Mapping the BKCa channel's "Ca^{2+} bowl." Side-chains essential for Ca^{2+} sensing. *J. Gen. Physiol.* **123,** 475–489
39. Javaherian, A. D., Yusifov, T., Pantazis, A., Franklin, S., Gandhi, C. S., and Olcese, R. (2011) Metal-driven operation of the human large-conductance voltage- and Ca^{2+}-dependent potassium channel (BK) gating ring apparatus. *J. Biol. Chem.* **286,** 20701–20709
40. Mannuzzu, L. M., Moronne, M. M., and Isacoff, E. Y. (1996) Direct physical measure of conformational rearrangement underlying potassium channel gating. *Science* **271,** 213–216
41. Cha, A., and Bezanilla, F. (1997) Characterizing voltage-dependent conformational changes in the Shaker K^+ channel with fluorescence. *Neuron* **19,** 1127–1140
42. Gandhi, C. S., and Olcese, R. (2008) The voltage-clamp fluorometry technique. In *Methods in Molecular Biology, Potassium Channels* (Lippiat, J. D., ed) Humana Press, Totowa, NJ
43. Escobar, A. L., Velez, P., Kim, A. M., Cifuentes, F., Fill, M., and Vergara, J. L. (1997) Kinetic properties of DM-nitrophen and calcium indicators. Rapid transient response to flash photolysis. *Pflugers Arch.* **434,** 615–631
44. Ellis-Davies, G. C. (2003) Development and application of caged calcium. *Methods Enzymol.* **360,** 226–238
45. Faas, G. C., Karacs, K., Vergara, J. L., and Mody, I. (2005) Kinetic properties of DM-nitrophen binding to calcium and magnesium. *Biophys. J.* **88,** 4421–4433
46. Ellis-Davies, G. C. (2007) Caged compounds. Photorelease technology for control of cellular chemistry and physiology. *Nat. Methods* **4,** 619–628
47. Wallner, M., Meera, P., Ottolia, M., Kaczorowski, G. J., Latorre, R., Garcia, M. L., Stefani, E., and Toro, L. (1995) Characterization of and modulation by a β-subunit of a human maxi KCa channel cloned from myometrium. *Receptors Channels* **3,** 185–199
48. Savalli, N., Kondratiev, A., de Quintana, S. B., Toro, L., and Olcese, R. (2007) Modes of operation of the BKCa channel β2 subunit. *J. Gen. Physiol.* **130,** 117–131
49. Haug, T., Sigg, D., Ciani, S., Toro, L., Stefani, E., and Olcese, R. (2004) Regulation of K^+ flow by a ring of negative charges in the outer pore of BKCa channels. Part I: Aspartate 292 modulates K^+ conduction by external surface charge effect. *J. Gen. Physiol.* **124,** 173–184
50. Stefani, E., and Bezanilla, F. (1998) Cut-open oocyte voltage-clamp technique. *Methods Enzymol.* **293,** 300–318
51. Pantazis, A., Kohanteb, A. P., and Olcese, R. (2010) Relative motion of transmembrane segments S0 and S4 during voltage sensor activation in the human BK(Ca) channel. *J. Gen. Physiol.* **136,** 645–657
52. Moczydlowski, E., and Latorre, R. (1983) Gating kinetics of Ca^{2+}-activated K^+ channels from rat muscle incorporated into planar lipid bilayers. Evidence for two voltage-dependent Ca^{2+} binding reactions. *J. Gen. Physiol.* **82,** 511–542
53. Sun, X. P., Yazejian, B., and Grinnell, A. D. (2004) Electrophysiological properties of BK channels in *Xenopus* motor nerve terminals. *J. Physiol.* **557,** 207–228
54. Sy, T., Grinnell, A. D., Peskoff, A., and Yazejian, B. (2010) Monitoring transient Ca^{2+} dynamics with large-conductance Ca^{2+}-dependent K^+ channels at active zones in frog saccular hair cells. *Neuroscience* **165,** 715–722
55. Sweet, T. B., and Cox, D. H. (2008) Measurements of the BKCa channel's high-affinity Ca^{2+} binding constants. Effects of membrane voltage. *J. Gen. Physiol.* **132,** 491–505
56. Yang, J., Krishnamoorthy, G., Saxena, A., Zhang, G., Shi, J., Yang, H., Delaloye, K., Sept, D., and Cui, J. (2010) An epilepsy/dyskinesia-associated mutation enhances BK channel activation by potentiating Ca^{2+} sensing. *Neuron* **66,** 871–883
57. Niu, X., and Magleby, K. L. (2002) Stepwise contribution of each subunit to the cooperative activation of BK channels by Ca^{2+}. *Proc. Natl. Acad. Sci. U.S.A.* **99,** 11441–11446
58. Sheng, J. Z., Weljie, A., Sy, L., Ling, S., Vogel, H. J., and Braun, A. P. (2005) Homology modeling identifies C-terminal residues that contribute to the Ca^{2+} sensitivity of a BKCa channel. *Biophys. J.* **89,** 3079–3092
59. Fettiplace, R., and Fuchs, P. A. (1999) Mechanisms of hair cell tuning. *Annu. Rev. Physiol.* **61,** 809–834
60. Hu, H., Shao, L. R., Chavoshy, S., Gu, N., Trieb, M., Behrens, R., Laake, P., Pongs, O., Knaus, H. G., Ottersen, O. P., and Storm, J. F. (2001) Presynaptic Ca^{2+}-activated K+ channels in glutamatergic hippocampal terminals and their role in spike repolarization and regulation of transmitter release. *J. Neurosci.* **21,** 9585–9597
61. Salkoff, L., Butler, A., Ferreira, G., Santi, C., and Wei, A. (2006) High-conductance potassium channels of the SLO family. *Nat. Rev. Neurosci.* **7,** 921–931
62. Braun, M., Ramracheya, R., Bengtsson, M., Zhang, Q., Karanauskaite, J., Partridge, C., Johnson, P. R., and Rorsman, P. (2008) Voltage-gated ion channels in human pancreatic β-cells. Electrophysiological characterization and role in insulin secretion. *Diabetes* **57,** 1618–1628
63. Wu, R. S., and Marx, S. O. (2010) The BK potassium channel in the vascular smooth muscle and kidney. α- and β-subunits. *Kidney Int.* **78,** 963–974
64. Cui, J., Yang, H., and Lee, U. S. (2009) Molecular mechanisms of BK channel activation. *Cell Mol. Life Sci.* **66,** 852–875
65. Horrigan, F. T., and Ma, Z. (2008) Mg^{2+} enhances voltage sensor/gate coupling in BK channels. *J. Gen. Physiol.* **131,** 13–32
66. Du, W., Bautista, J. F., Yang, H., Diez-Sampedro, A., You, S. A., Wang, L., Kotagal, P., Lüders, H. O., Shi, J., Cui, J., Richerson, G. B., and Wang, Q. K. (2005) Calcium-sensitive potassium channelopathy in human epilepsy and paroxysmal movement disorder. *Nat. Genet.* **37,** 733–738
67. Long, S. B., Tao, X., Campbell, E. B., and MacKinnon, R. (2007) Atomic structure of a voltage-dependent K^+ channel in a lipid membrane-like environment. *Nature* **450,** 376–382
68. Liu, G., Niu, X., Wu, R. S., Chudasama, N., Yao, Y., Jin, X., Weinberg, R., Zakharov, S. I., Motoike, H., Marx, S. O., and Karlin, A. (2010) Location of modulatory beta subunits in BK potassium channels. *J. Gen. Physiol.* **135,** 449–459